Intermetallics 18 (2010) 1930–1935

Contents lists available at ScienceDirect

Intermetallics

journal homepage: www.elsevier.com/locate/intermet

Mechanical responses of Mg-based bulk metallic glasses

S.-R. Jian [a,*], J.-B. Li [a], K.-W. Chen [b], Jason S.-C. Jang [c], J.-Y. Juang [d], P.-J. Wei [e], J.-F. Lin [b,f]

[a] Department of Materials Science and Engineering, I-Shou University, Kaohsiung 840, Taiwan
[b] Department of Mechanical Engineering, National Cheng Kung University, Tainan 701, Taiwan
[c] Department of Mechanical Engineering; Institute of Materials Science & Engineering, National Central University, Chung-Li 320, Taiwan
[d] Department of Electrophysics, National Chiao Tung University, Hsinchu 300, Taiwan
[e] Institute of Nanotechnology and Microsystems Engineering, National Cheng Kung University, Tainan 701, Taiwan
[f] Center for Micro/Nano Science and Technology, National Cheng Kung University, Tainan 701, Taiwan

ARTICLE INFO

Article history:
Received 17 November 2009
Received in revised form
9 March 2010
Accepted 22 March 2010
Available online 13 April 2010

Keywords:
B. Glasses, metallic
E. Mechanical properties, theory
F. Mechanical testing
F. Electron microscopy, transmission

ABSTRACT

In this study, the mechanical responses of the bonded interface method derived $Mg_{58}Cu_{28.5}Gd_{11}Ag_{2.5}$ bulk metallic glasses (BMG) under the micro-/nano-indentation are investigated. A modified expanding cavity model is developed to analyze the morphological observations of shear band by Vickers indentation. Results indicate that the radius ratio of any two adjacent shear band circles is approximately constant. The ratio of the shear band deformation zone to the contact radius induced by indentation is also a constant, which depends on the constraint factor (the ratio of hardness to yield strength) of the material. The features predicted by the present model are consistent with the results obtained from the indentation experiments, indicating the validity of the expanding cavity model for describing the mechanical behaviors of the BMG materials. The cross-sectional transmission electron microscopy (XTEM) observations reveal that the terraced shear bands are formed on the interface of the bonded Mg-based BMG. The microstructures for the Vickers indentation-induced terraced shear bands are also discussed.

1. Introduction

Recently, bulk metallic glasses (BMGs) have attracted rapidly increasing attention due to their importance in understanding the fundamental science involved as well as the potential engineering applications [1]. The interrelations between the microstructure and material properties of amorphous alloys, such as high strength, large elastic limit, and high corrosion resistance are quite different from those prevailing in crystalline alloys [2–5]. The excellent physical, chemical, and mechanical characteristics exhibited in BMGs have brought about high potential of using them as engineering or structural materials. However, monolithic BMGs have been confronting a fatal problem of brittleness at temperatures below the glass transition temperature (T_g). The localized shear bands are formed in BMGs at room temperature because of the highly concentrate deformation induced by pressure [6,7]. The shear band zone exhibits strain softening, which leads to further plastic deformation and ultimate fracture [8–10]. These drawbacks have limited the applications of BMGs as engineering materials.

To estimate the shear band emission of BMGs, micro/nano-indentation methods have been widely used to measure the mechanical properties and elastic/plastic responses of BMGs. Previously studies have reported that the formation of shear bands underneath the indentation cavity created by Vickers and spherical indentation were frequently exhibiting morphologies of semi-circular shape [6–8]. Two primary types of shear band were observed in the deformation zone: primary shear band (PSB) and secondary shear band (SSB) [10–12]. In addition, the load-displacement curve exhibits the displacement bursts, known as serrations or pop-in events, in the course of the indentation process [13–16]. The size of pop-ins was found to increase with indentation depth but decrease with the indentation loading rate. The pop-in events, thus, were believed to be closely related to the emission of shear bands during indentation process [17,18].

In the present study, the mechanical characteristics of $Mg_{58}Cu_{28.5}Gd_{11}Ag_{2.5}$ BMG [19,20], an alloy with high glass forming ability, fabricated by using a bonded interface method was investigated using indentation techniques. A modified Johnson's expanding cavity model [21] was developed to describe the relationship between the ratios between the radii of any two adjacent shear band circles. The ratio of deformation zone to contact radius of an indentation cavity can also be obtained using the present

* Corresponding author. Tel.: +886 7 6577711x3130; fax: +886 7 6578444.
E-mail address: srjian@gmail.com (S.-R. Jian).

0966-9795/$ – see front matter © 2010 Elsevier Ltd. All rights reserved.
doi:10.1016/j.intermet.2010.03.034

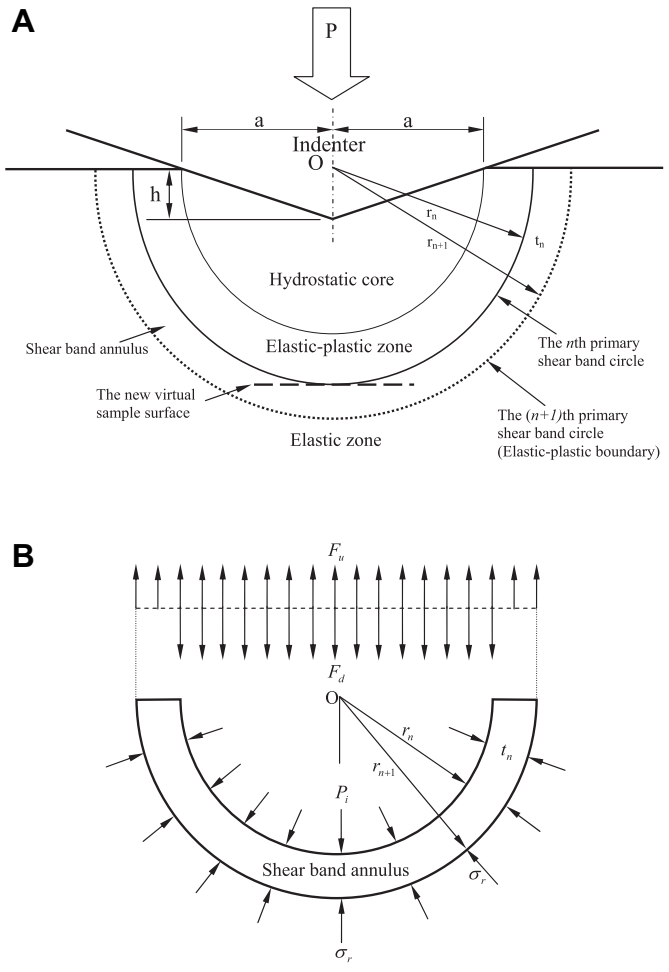

Fig. 1. (a) Schematic diagram of the expanding cavity model of the elastic-plastic region induced by an indentation on a BMG surface. (b) Free body diagram of a shear band annulus.

model, provided the hardness and yield strength of the specimen are available. The experimental results obtained from the microstructural features of the indentation-induced shear bands produced by Vickers indenter have largely confirmed the predictions given by the modified expanding cavity model. The microstructure analyses reported were carried out by using the dual beam focused ion beam (DB-FIB) and transmission electron microscopy (TEM) techniques.

2. Experimental details

The $Mg_{58}Cu_{28.5}Gd_{11}Ag_{2.5}$ BMG rods with diameter of 4 mm were prepared by injection casting method as had been described previously [19]. The amorphous structure of these as-casted Mg-based BMG specimen was verified by X-ray diffractometer (XRD, Scintag X-400®) with a monochromatic Cu-Kα radiation. Differential scanning calorimetry (DSC) measurement was applied to reveal the glass transition temperature (T_g) and the crystallization temperature (T_x) of the Mg-based material. The DSC measurements were carried out in the temperature range of 350–550 K with a heating rate of 20 K/min. Indentation experiments were performed at room temperature (22 °C) using a nanoindenter (MTS Nano Indenter XP, USA) for nanoindentation tests and a Vickers indenter for microindentation tests. MTS nanoindentation tests were performed under continuous stiffness mode (CSM) with a strain rate of 0.05/s and maximum indentation depth of 2500 nm. The radius of the Berkovich indenter

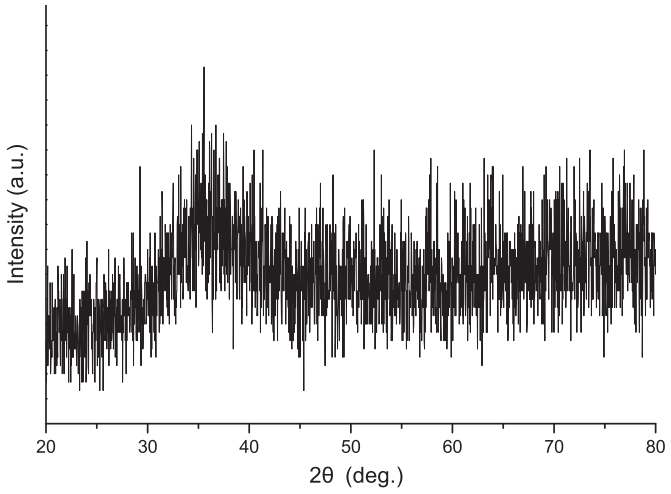

Fig. 2. XRD pattern of as-cast $Mg_{58}Cu_{28.5}Gd_{11}Ag_{2.5}$ alloy.

tip is about 150 nm. The thermal drift was controlled to be less than 0.15 nm/s. In order to reveal the morphology of the shear band beneath the indentation cavity the bonded interface technique was employed to prepare specimens for Vickers microindentation tests. The bonded interfaces were polished to a mirror finish and mounted immediately to prevent the specimens from oxidation. In the Vickers indentation tests, a maximum load of 500 gf (approximately 4900 mN) and a loading time of 15 s were applied. The cross-sectional transmission electron microscopy (XTEM) specimen preparation were performed using dual beam focused ion beam (DB-FIB) system with Ga ions source. Prior to the ion-milling process, a 1.5-μm thick carbon layer was deposited as the protective layer to protect the original microstructure from damage caused by Ga ions bombardment. The microstructures of the shear bands were, then, examined by using the scanning electron microscopy (SEM) and TEM (FEI, $G^2$20 S-Twin).

3. Model methodology

During the indentation process, it has been established that the dominant deformation mechanism at room temperature is the

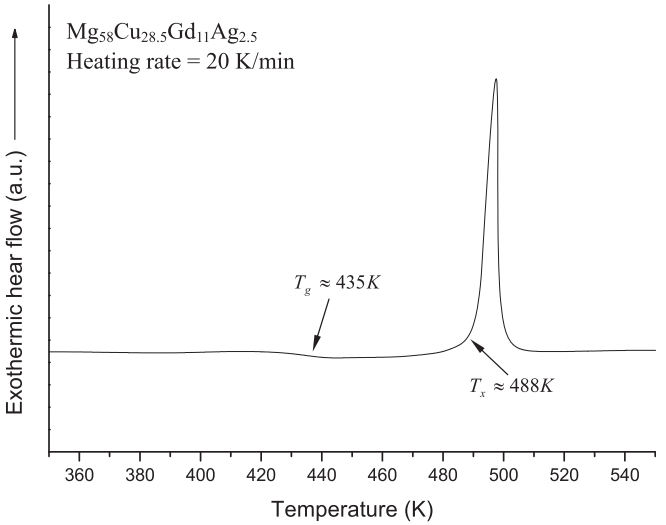

Fig. 3. DSC trace of as-cast $Mg_{58}Cu_{28.5}Gd_{11}Ag_{2.5}$ alloy. The heating rate is controlled to be 20 K/min. The glass transition temperature and crystallization temperature are obtained 435 K and 488 K, respectively.

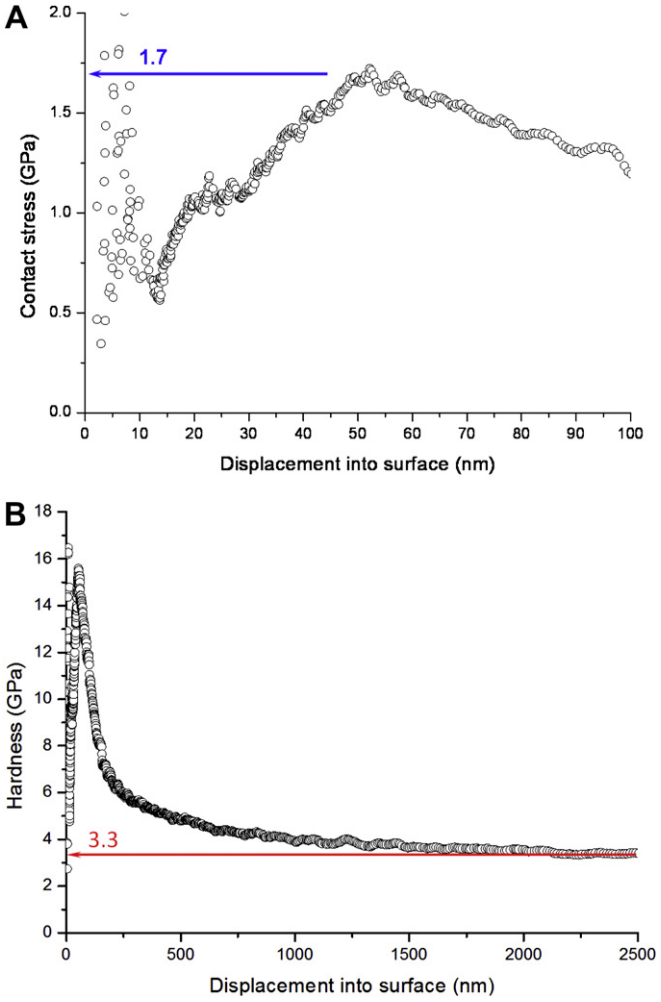

Fig. 4. MTS nanoindentation results for as-cast $Mg_{58}Cu_{28.5}Gd_{11}Ag_{2.5}$ alloy. (a) The normal contact stress as a function of indentation depth. (b) The hardness as a function of indentation depth.

formation of shear bands. Previous studies [6–12] have further indicated that the indentation-induced shear bands generated by Vickers indenters can be approximately fitted by circles with various radii. It is conceived that, due to the isotropic nature of BMGs, the shear bands follow closely with the semi-circular stress contours beneath the indentation cavity. Nevertheless, direct comparisons between the actual nanoindentation-induced shear band morphologies with the theoretical expectations are lacking. Therefore, a combination of indentation, SEM and FIB techniques together with the expanding cavity model [21] are carried out to investigate the morphological evolutions of Vickers indentation-induced shear bands in Mg-based BMG materials.

A schematic diagram of the expanding cavity model of the elastic-plastic region induced by indentations is shown in Fig. 1(a). During the indentation process, the outermost shear band circle can be viewed as the elastic-plastic boundary in the cavity model. The shear band circles are constantly produced with the increasing indentation load (P). In Fig. 1(a), the contact radius is represented as a, and the indentation depth is h. Very recently, Yoo and Jang [10] and Xie and George [11] proposed that a pile-up effect may play a role in BMG indentation experiments. Nevertheless, we note that, compared to the scale of an indentation cavity, the pile-up effect is too small and, thus, is neglected in the present analysis. Fig. 1(b) shows a free body diagram of a shear band annulus between the (n)th and the $(n+1)$th shear band circles. The thickness of annulus is

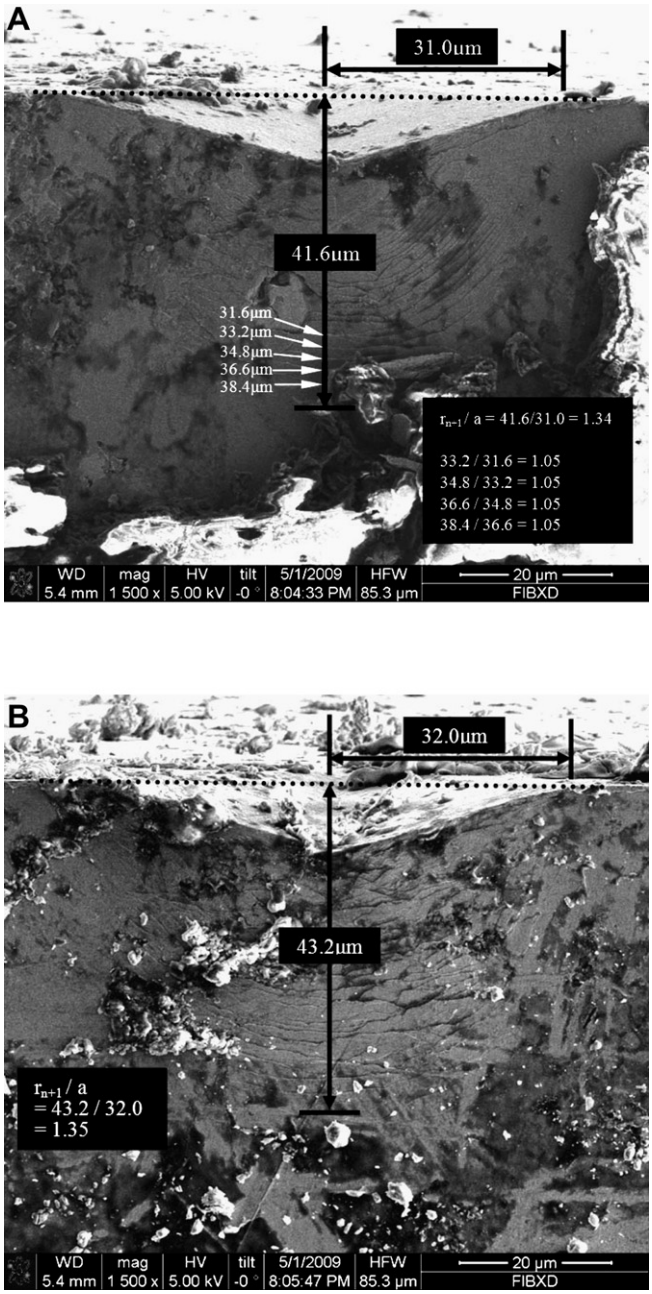

Fig. 5. The SEM images of Vickers indentations. The ratios of shear band deformation zone to the contact radius of these indentations are approximately a constant value of 1.33.

denoted as t_n, which is called the shear band spacing. Consequently, the relationship between the (n)th and the $(n+1)$th shear band circle can be written as:

$$r_{n+1} = r_n + t_n \tag{1}$$

where r_n and r_{n+1} are the radius of the (n)th and the $(n+1)$th shear band circles, respectively. Since r_{n+1} is defined as the radius of outermost shear band circle, which is the latest formed elastic-plastic boundary, r_{n+1} also represents the radius of deformation zone induced by indentations.

In Fig. 1(b), the stresses σ_r acting at the outer surface of the $(n+1)$th shear band circle can be integrated to obtain an upward force F_u in the vertical direction. Similarly, the stress P_i acting on the inner surface of the (n)th shear band circle produces the same effect as that of the downward force F_d in the vertical direction.

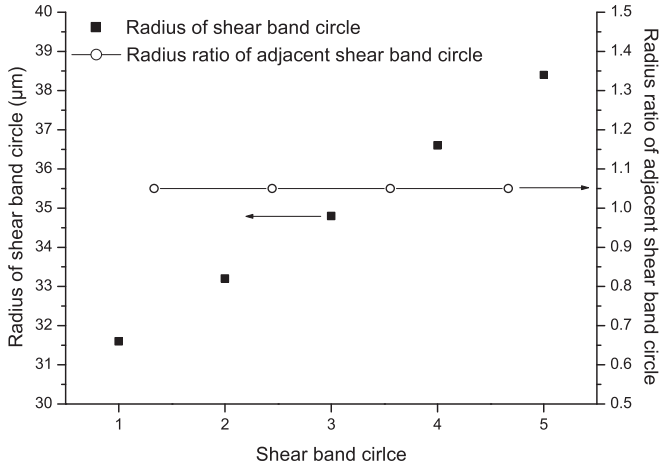

Fig. 6. The radii and radius ratio as a function of shear band circle obtained from Fig. 6(a).

Considering the force balance in the vertical direction of the shear band annulus ($F_u = F_d$), the equilibrium equation can be written as:

$$\frac{P_i}{\sigma_r} = \left(\frac{r_n + t_n}{r_n}\right)^2 \tag{2}$$

Defining P_m as the mean contact pressure acting on the projection area of the indentation cavity, as shown in Fig. 1(a). In this study, the microindentations were performed using a Vickers indenter with a half-diagonal length of a, one obtains $F_d = P_m 2a^2 = \pi r_n^2 P_i$. According to the Johnson's cavity model in contact mechanics [21], the relationship between the radius stress σ_r acting on the outer elastic-plastic boundary and the yield strength Y can be written as $\sigma_r = 2Y/3$. Then, the mean contact pressure P_m is equal to the hardness (H) of specimen when the material starts to yield. Substitution of P_i and σ_r into Eq. (2) gives:

$$\frac{H}{Y} = \frac{\pi}{3}\left(\frac{r_n}{a}\right)^2 \left(\frac{r_n + t_n}{r_n}\right)^2 = \frac{\pi}{3}\left(\frac{r_{n+1}}{a}\right)^2 \tag{3}$$

Generally, the value of H/Y is called the "constraint factor, C_c". Since the constraint factor on the left-hand side of Eq. (3) is a constant, the value of r_{n+1}/a on the right-hand side of Eq. (3) must be a constant, too. This result suggests that, for an isotropic BMG material, the ratio of the deformation zone to the contact radius of an indentation cavity should be a constant value, as well. The validity of this conclusion will be discussed later.

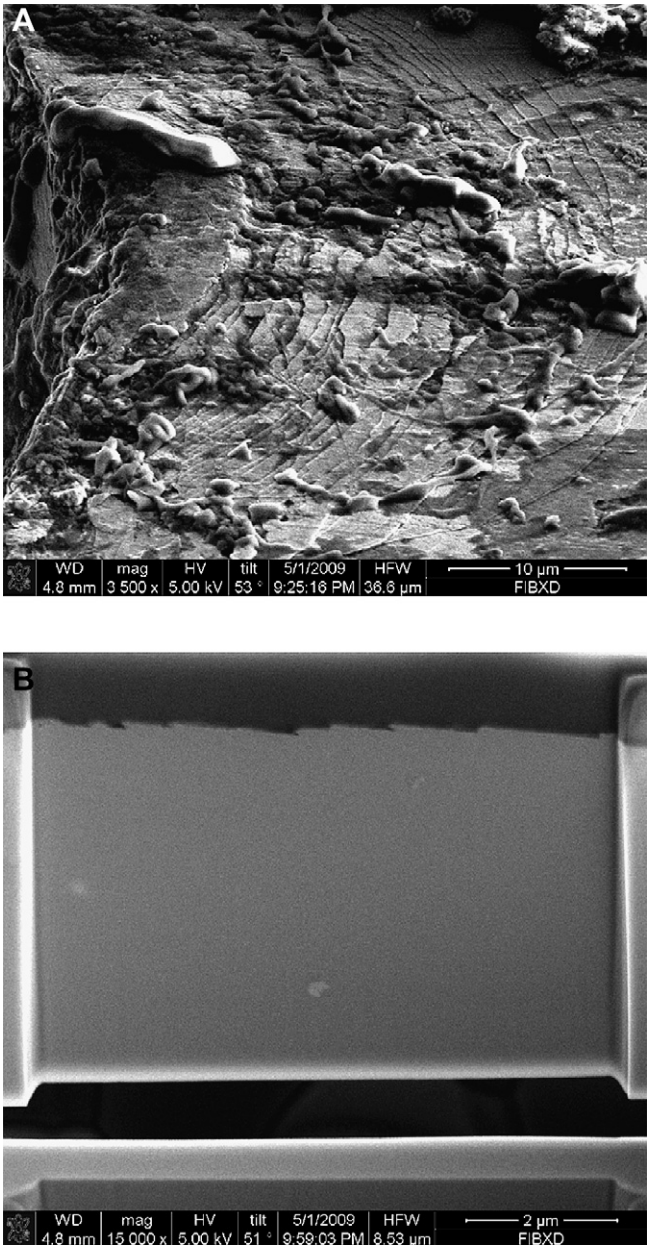

Fig. 7. (a) The morphological picture of Vickers indentation-induced shear bands and (b) the cross-sectional view of shear band circles are obtained using FIB-SEM.

4. Results and discussion

The XRD pattern of the as-cast $Mg_{58}Cu_{28.5}Gd_{11}Ag_{2.5}$ alloy is displayed in Fig. 2. The pattern was recorded from the top surface of the specimen with the 2θ angle being scanned in the range of$20^\circ \le 2\theta \le 80^\circ$. It is evident from Fig. 2 that no apparent crystalline peak except for a broadened diffraction peak is detected, indicating that the specimen is fully amorphous.

The DSC trace of the as-cast $Mg_{58}Cu_{28.5}Gd_{11}Ag_{2.5}$ alloy is displayed in Fig. 3. It can be seen that a clear glass transition temperature ($T_g \sim 435$ K) and a sharp peak of the crystallization temperature ($T_x \sim 497$ K) are evident for the Mg-based BMG investigated in the present study. The width of the supercooled liquid region ($\Delta T_x = T_x - T_g$) was thus determined to be 62 K. These results confirmed the high glass forming ability of the present Mg-based BMGs.

Fig. 4 shows the nanoindentation results for the as-cast $Mg_{58}Cu_{28.5}Gd_{11}Ag_{2.5}$ alloy. The normal contact stress as a function of indentation depth is displayed in Fig. 4(a). The contact stress was determined by the load applied on the sample divided by the projection of the contact area, namely $\sigma = P/A_{contact}$. Due to the lack of dislocation-mediated crystallographic slip, the results clearly display a marked scattering feature in the contact stress for the first 15 nm of indentation, which is very different from those observed in crystalline materials [22]. We suspect that it might due to the adjustments of the local short-range and medium range order structures inherent in the glassy state [23]. Alternatively, it could be also reflecting the deformation resulting from the initiation of the first shear band, which is believed to be only ~10 nm [23]. The data then exhibit a clear turn in the trend at an indentation depth of about 50 nm. The yield strength was thus determined to be about $Y = 1.7$ GPa from Fig. 4(a). It should be noted that the yield strength obtained using indentation method is higher than the value

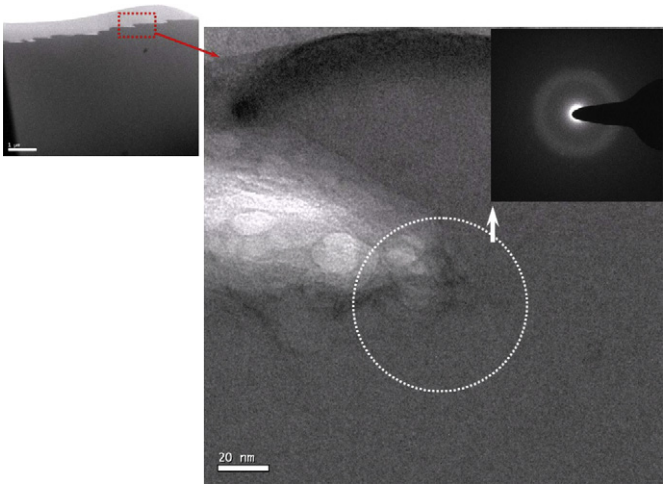

Fig. 8. XTEM images of the same area in Fig. 8(b). An enlarged image of the terraced shear band on the bonded interface of Mg-based BMG is observed.

obtained using tension and compression methods, presumably due to the more microscopic properties are being probed by the indentation test. The variation of hardness with the increasing indentation depth for the as-cast $Mg_{58}Cu_{28.5}Gd_{11}Ag_{2.5}$ alloy is illustrated in Fig. 4(b). The curve of hardness decreases asymptotically to a constant value of 3.3 GPa after the initial sharp rise for indentation depth below 50 nm or so. Therefore, this value is defined as the hardness ($H = 3.3$ GPa) of the sample. The constraint factor of the present Mg-based BMG is then determined to be $H/Y = C_c = 1.94$. Substituting the above constraint factor into Eq. (3), one obtains the ratio of deformation zone to contact radius to be $r_{n+1}/a = 1.36$. This result reveals that during the indentation process on an isotropic amorphous alloy, the ratio between the shear band deformation zone and the contact radius should be a fixed value depending on the hardness and yield strength (or constraint factor) of the material.

The deformation morphologies of two different Vickers indentation-induced shear bands observed by SEM are displayed in Fig. 5. In these two images the semi-circular shear bands are clearly visible and the contact radii and shear band deformation zones can be easily measured directly from Fig. 5(a) and (b). In addition, the ratios of shear band deformation zone to contact radius (r_{n+1}/a) for Fig. 5 were calculated to be 1.34 and 1.35, respectively. The results show that these ratios are consistent with the predicted value of 1.36 by the proposed model. In Fig. 5(a), the semi-circular shear bands are smoother than that in Fig. 5(b). These shear band circles are helpful for estimating the radius ratio in Eq.(2). Five adjacent shear band circles far from the tip of indentation cavity were specifically labeled in Fig. 5(a) to estimate the radius of each semi-circular shear band. The radii and radius ratios of these shear band circles are displayed in Fig. 6. It is evident that the radius ratio of any two adjacent shear band circles is almost constant with a value of 1.05. This result indicates that the term of radius ratio (r_{n+1}/r_n) in Eq. (3) can be defined as a constant value C and the radii of shear band circles are geometric series with a common ratio C, namely, $r_{n+1}/r_n = C$, and $r_{n+1} = Cr_n$. Substituting the above expression into Eq. (1) gives:

$$t_n = (C-1)r_n \tag{4}$$

Eq. (4) indicates that the shear band spacing, t_n, is linearly proportional to the radius of shear band circle. This is in good agreement with experimental results reported in the previous studies [8,10–12], which showed that the shear band spacing between the semi-circular bands increases with the indentation depth.

The microstructure of the Vickers indentation-induced shear bands for the present Mg-based BMG was further examined by SEM and XTEM techniques. A series of semi-circular shear band induced by Vickers indentation on the bonded interface of the sample is displayed in Fig. 7. It reveals that the bonded interface is no longer smooth, but in the form of terraces between the shear band circles. These terraces exhibit on the bonded interface were due to the shear band sliding induced by indentation, as displayed in Fig. 7(a). Moreover, the cross-sectional view of the terraced shear bands is shown in Fig. 7(b). In order to have a closer look at the terraced shear band, Fig. 8 shows an enlarged XTEM picture. It can be seen that the shear bands exhibit on the bonded interface do not expand into the material beneath the bonded interface. This may due to the thickness of TEM sample or the local melting induced by ion bombardment during FIB sampling process. However, the observation reveals that the present Mg-based BMG material has no crystallization and remains amorphous phase after shear sliding deformation, as is confirmed by the select area diffraction pattern displayed in the inset of Fig. 8.

5. Conclusions

In summary, the modified expanding cavity model developed for Vickers indentation-induced shear bands appears to successfully describing the deformation behaviors of the Mg-based BMGs. The experimental results obtained from the Vickers indentation evidently confirmed the model predictions. Namely, the ratio of the shear bands deformation zone to the contact radius (a) depends sorely on the constraint factor (H/Y) of the specimen; the radii of shear band circles are generally in a form of geometric series with a common ratio of C; and the spacing of shear bands between two adjacent shear band circles is linearly proportional to the radius of shear band circle. From the XTEM observations, the terraced shear bands do not expand further into the material beneath the bonded interface. Selected area diffraction pattern reveals that the microstructures near the Vickers indentation-induced terraced shear bands remain amorphous. No crystallization occurs during shear band sliding deformation induced by indentation in the present Mg-based BMG materials.

Acknowledgements

This work was partially supported by the National Science Council of Taiwan, under Grant No.: NSC 97-2112-M-214-002-MY2, NSC 95–2210-E-214–015-MY3, and NSC 98-2221-E-008-116-MY3. JYJ is partially supported by the MOE-ATU program operated at NCTU.

References

[1] Inoue A, Zhang T, Masumoto T. Mater Trans JIM 1990;31:104.
[2] Inoue A. Acta Mater 2000;48:279.
[3] Scully JR, Gebert A, Payer JH. J Mater Res 2007;22:303.
[4] Inoue A, Shen BL, Koshiba H, Kato H, Yavari AR. Acta Mater 2004;52:1631.
[5] Eckert J, Das J, Pauly S, Duhamel C. J Mater Res 2007;22:285.
[6] Jana S, Bhowmick R, kawamura Y, Chattopadyay K, Ramamurty U. Intermetallics 2004;12:1097.
[7] Jana S, Ramamurty U, Chattopadhyay K, Kawamura Y. Mater Sci Eng 2004;A 375-377:1191.
[8] Xing D, Zhang T, Li W, Wei B. J. Alloys Compd 2007;433:318.
[9] Bei H, Xie S, George EP. Phys Rev Lett 2006;96:105503.
[10] Yoo BG, Jang J. J Phys D Appl Phys 2008;41:074017.
[11] Xie S, George EP. Acta Mater 2008;56:5202.
[12] Ramamurty U, Jana S, Kawamura Y, Chattopadhyay K. Acta Mater 2005;53:705.

[13] Song SX, Jang JSC, Nieh TG. Intermetallics 2008;16:676.
[14] Burgess T, Laws KJ, Ferry M. Acta Mater 2008;56:4829.
[15] Liu L, Chan KC. Mater Lett 2005;59:3090.
[16] Wang L, Song SX, Nieh TG. App Phys Lett 2008;92:101925.
[17] Schuh CA, Nieh TG. Acta Mater 2003;51:87.
[18] Schuh CA, Nieh TG. J Mater Res 2004;19:46.
[19] Jang JSC, Ciou JY, Hung TH, Huang JC, Du XH. Appl Phys Lett 2008;92:011930.
[20] Jang JSC, Jian SR, Li TH, Huang JC, Tsao Chi YA, Liu CT. J Alloys Compd 2009;485:290.
[21] Johnson KL. Contact mechanics. New York: Cambridge; 1989. p. 171–179.
[22] Jian SR, Juang JY, Lai YS. J Appl Phys 2008;103:033503.
[23] Yavari AR, Lewandowski JJ, Eckert J. MRS Bull 2007;32:635.